

How to observe the giant thermal effect in the Casimir force for graphene systems

G. Bimonte,^{1,2} G. L. Klimchitskaya,^{3,4} and V. M. Mostepanenko^{3,4,5}

¹*Dipartimento di Fisica E. Pancini, Università di Napoli Federico II,
Complesso Universitario MSA, Via Cintia, I-80126 Napoli, Italy*

²*INFN Sezione di Napoli, I-80126, Napoli, Italy*

³*Central Astronomical Observatory at Pulkovo of the Russian
Academy of Sciences, Saint Petersburg, 196140, Russia*

⁴*Institute of Physics, Nanotechnology and Telecommunications,
Peter the Great Saint Petersburg Polytechnic University, Saint Petersburg, 195251, Russia*

⁵*Kazan Federal University, Kazan, 420008, Russia*

Abstract

A differential measurement scheme is proposed which allows for a clear observation of the giant thermal effect for the Casimir force, that was recently predicted to occur in graphene systems at short separation distances. The difference among the Casimir forces acting between a metal-coated sphere and the two halves of a dielectric plate, one uncoated and the other coated with graphene, is calculated in the framework of the Dirac model using the rigorous formalism of the polarization tensor. It is shown that in the proposed configuration both the difference among the Casimir forces and its thermal contribution can be easily measured using already existing experimental setups. An observation of the giant thermal effect should open opportunities for modulation and control of dispersion forces in micromechanical systems based on graphene and other novel 2D-materials.

I. INTRODUCTION

During the last few years graphene attracted a widespread attention in physics, material science and nanotechnological applications due to its unusual mechanical, optical and electrical properties [1–4]. These properties originate from the fact that graphene is a two-dimensional layer of carbon atoms organized in a honeycomb crystal lattice. At low energies the quasiparticles in graphene are massless (or almost massless) charged fermions described by the Dirac equation. Interest in graphene and relativistic Dirac-like systems in condensed matter physics further increased after other two-dimensional honeycomb materials called silicene, germanene and stanene (which are 2D allotropes of Si, Ge and Sn) have been discovered [5–7].

Another much studied interdisciplinary subject is represented by the fluctuation-induced (dispersion) forces acting between two microparticles, a material surface and a microparticle, and between two closely spaced material surfaces. These forces are of entirely quantum origin. For separations between the interacting bodies smaller than a few nanometers these interactions have a nonrelativistic character and are commonly known as *van der Waals forces* [8]. At larger separations relativistic effects come into play and the name *Casimir forces* [9] is most often used. Even though the energies associated with these forces usually represent just a small contribution to the total free energy of the respective material systems, they are presently considered to be a crucial ingredient for a qualitatively correct and quantitatively accurate description of the binding properties of materials [10]. This is the reason why van der Waals and Casimir forces are actively studied both experimentally and theoretically (see Refs. [11–13] for a review). In so doing, puzzling findings concerning the role of dissipation of free charge carriers in metals have been reported [14–19] and important applications of dispersion forces in micromechanical systems [20–22] and nanochips [23] have been proposed.

In view of the universal character of dispersion forces, it is widely acknowledged that their role is also important for closely spaced graphene sheets, graphene-coated substrates, and graphene and regular 3D-materials. The van der Waals and Casimir forces in microsystems involving graphene have already been studied using a variety of theoretical approaches [24–34]. In the framework of the Dirac model [1–4], the natural description of the Casimir force in graphene systems, based on the first principles of quantum electrodynamics at nonzero

temperature, is provided by the formalism of the polarization tensor in (2+1)-dimensional space-time [35–41]. In the one-loop approximation this approach is indeed equivalent [42] to the formalism of density-density correlation functions in the random-phase approximation. Using the latter approach, it was discovered [24] that differently from 3D-materials the Casimir force for graphene systems displays a giant thermal effect, which provides a very large contribution to the force magnitude at relatively small separations of about 150 nm. This is surprising if one considers that for 3D-materials the thermal effect becomes dominant only for separations larger than the thermal length $\lambda_T = \hbar c / (k_B T)$ (about $7 \mu\text{m}$ for room temperature), where the magnitude of the Casimir force is anyhow very small. Detailed investigations of the thermal effect in graphene systems [43, 44] demonstrated that it can be harnessed to modulate and control the strength of the Casimir force. In spite of its importance and unusual features, this thermal effect has not been measured yet.

In this paper, we propose an experimental approach allowing for an unambiguous measurement of the giant thermal effect in the Casimir force between a Au-coated sphere and a graphene-coated Si substrate made of dielectric Si. According to our results, this can be achieved by measuring the *difference* among the Casimir forces between a Au-coated sphere and the two halves of a Si plate, one of which is coated and the other is uncoated with a graphene sheet (see Fig. 1). A conceptually similar differential approach has been successfully used in the past to determine the role of relaxation of free charge carriers in the Casimir force between metallic test bodies [19, 45–47] and for constraining hypothetical corrections of Yukawa type to Newton’s law of gravitation [48, 49]. The experimental setups used in these investigations achieved a force sensitivity of a fraction of 1 fN at room temperature. Below we show that at separations of 100 nm, 1 and $1.5 \mu\text{m}$ our measurement scheme leads to differential Casimir forces equal to approximately 2.3 pN, 18.5 fN, and 8.1 fN, respectively. At the same separations, according to our results, the thermal effect in graphene contributes 1.5 pN, 17.5 fN, and 7.8 fN, respectively. Thus, this effect should be easily measurable over the entire separation range from 100 nm to $1.5 \mu\text{m}$ taking into account the sensitivity of existing experimental setups.

The structure of the paper is as follows. In Sec. II we describe the proposed experimental setup and show how to compute the Casimir force difference between the two halves of the Si plate on the basis of the formalism of the polarization tensor for graphene. In Sec. III we report the results of our numerical computations. Section IV presents our conclusions and

an outline for future work.

II. EXPERIMENTAL SCHEME AND GENERAL FORMALISM

We consider the configuration of a Au-coated sphere of radius $R = 150 \mu\text{m}$ moving back and forth in vacuum at some height a above a plate made of dielectric Si (see Fig. 1). The thickness of the Au coating is chosen to be large enough (typically larger than a few tens of nanometers) that the sphere can be considered as made entirely of Au for the sake of computing the Casimir force. One half of the plate (the right half in Fig. 1) is coated with a graphene sheet. In a concrete experimental implementation, one could use a setup similar to those described in Refs. [19, 48, 49] employing a micromechanical torsional oscillator. Setups of this sort provide a direct measurement of the difference $F_{\text{diff}}(a, T)$ among the Casimir forces $F_{\text{Si}}(a, T)$ and $F_{\text{gr}}(a, T)$ acting, respectively, between a sphere and the uncoated and graphene-coated halves of a Si plate:

$$F_{\text{diff}}(a, T) = F_{\text{Si}}(a, T) - F_{\text{gr}}(a, T) . \quad (1)$$

The force difference F_{diff} at $T = 300 \text{ K}$ can be calculated using the Lifshitz formula [9, 50]. We assume that in Eq. (1) $F_{\text{Si}}(a, T)$ and $F_{\text{gr}}(a, T)$ are the forces acting on the sphere when its tip is placed above points that are respectively deep in the left and right halves of the Si plate, in such a way that the effect of the sharp boundary between the graphene-coated half and the uncoated half of the Si plate can be neglected. In practice, to achieve this, it is sufficient to place the sphere tip at a distance δ from the boundary that is larger than a few times the typical Casimir interaction radius $\rho = \sqrt{aR}$. Under these conditions the forces $F_{\text{gr}}(a, T)$ and $F_{\text{Si}}(a, T)$ become respectively undistinguishable from the forces that would act between the Au sphere and two distinct *homogeneous* Si plates, one fully covered with graphene and the other fully uncovered. The latter forces can be computed using the proximity force approximation [51] (in Refs. [52–55] it was rigorously proved that this approximation is sufficiently precise under the condition $a \ll R$). The result is

$$F_{\text{diff}}(a, T) = \frac{k_B T R}{4a^2} \sum_{l=0}^{\infty}{}' \int_{\zeta_l}^{\infty} y dy \sum_{\alpha} \ln \frac{1 - r_{\alpha}^{(1)}(i\zeta_l, y) r_{\alpha}^{(2)}(i\zeta_l, y) e^{-y}}{1 - r_{\alpha}^{(1)}(i\zeta_l, y) R_{\alpha}(i\zeta_l, y) e^{-y}}, \quad (2)$$

where k_B is the Boltzmann constant, the prime in the first summation sign means that the term with $l = 0$ is taken with weight $1/2$, $\zeta_l = 2a\xi_l/c$ are the dimensionless Matsubara

frequencies, the dimensional Matsubara frequencies being defined as $\xi_l = 2\pi k_B T l / \hbar$, and $y = 2a\sqrt{\mathbf{k}_\perp^2 + \xi_l^2/c^2}$ with the in-plane wave vector \mathbf{k}_\perp . The summation in α in Eq. (2) is over the transverse magnetic ($\alpha = \text{TM}$) and transverse electric ($\alpha = \text{TE}$) polarizations of the electromagnetic field. The reflection coefficients $r_\alpha^{(n)}$ on the boundaries between vacuum and Au ($n = 1$) or Si ($n = 2$) are given by

$$\begin{aligned} r_{\text{TM}}^{(n)}(i\zeta_l, y) &= \frac{\varepsilon_l^{(n)} y - k_l^{(n)}}{\varepsilon_l^{(n)} y + k_l^{(n)}}, \\ r_{\text{TE}}^{(n)}(i\zeta_l, y) &= \frac{y - k_l^{(n)}}{y + k_l^{(n)}}, \end{aligned} \quad (3)$$

where $\varepsilon_l^{(n)} \equiv \varepsilon^{(n)}(i\zeta_l)$ are the dielectric permittivities of Au and Si calculated at the imaginary Matsubara frequencies and $k_l^{(n)} = [y^2 + (\varepsilon_l^{(n)} - 1)\zeta_l^2]^{1/2}$. Finally, the reflection coefficients R_α on the boundaries between vacuum and the graphene-coated substrate (Si) can be expressed via the polarization tensor of graphene using the results of Refs. [37, 42, 56, 57]. The same results were obtained in Ref. [40] in the framework of another approach. In terms of the dimensionless variables one has [43]

$$R_{\text{TM}}(i\zeta_l, y) = \frac{\varepsilon_l^{(2)} y - k_l^{(2)} + y k_l^{(2)} (y^2 - \zeta_l^2)^{-1} \tilde{\Pi}_{00,l}}{\varepsilon_l^{(2)} y + k_l^{(2)} + y k_l^{(2)} (y^2 - \zeta_l^2)^{-1} \tilde{\Pi}_{00,l}}, \quad R_{\text{TE}}(i\zeta_l, y) = \frac{y - k_l^{(2)} - (y^2 - \zeta_l^2)^{-1} \tilde{\Pi}_l}{y + k_l^{(2)} - (y^2 - \zeta_l^2)^{-1} \tilde{\Pi}_l}. \quad (4)$$

Here, the dimensionless polarization tensor of graphene calculated at the Matsubara frequencies, $\tilde{\Pi}_{mn,l}$, is expressed via the dimensional one as $\tilde{\Pi}_{mn,l} \equiv \tilde{\Pi}_{mn}(\zeta_l, y) = 2a\Pi_{mn,l}/\hbar$ and the quantity $\tilde{\Pi}_l$ is defined by

$$\tilde{\Pi}_l \equiv (y^2 - \zeta_l^2) \tilde{\Pi}_{\text{tr},l} - y^2 \tilde{\Pi}_{00,l}, \quad (5)$$

where $\tilde{\Pi}_{\text{tr}}$ is the trace of the polarization tensor. Note that the polarization tensor describes the response of a physical system to an electromagnetic field. Because of this, it is immediately connected with physical quantities such as the dielectric permittivity [26, 42] and conductivity [58, 59] of graphene. For instance, the in-plane component of the nonlocal dielectric permittivity of graphene calculated at the imaginary Matsubara frequencies is given by [26, 42]

$$\varepsilon_l^\parallel = 1 + \frac{1}{2k_\perp \hbar} \Pi_{00,l}. \quad (6)$$

The dielectric permittivities of Au and dielectric Si entering Eqs. (3) and (4) are found from the optical data for the complex indices of refraction (see Refs. [60] and [61], respectively) using the Kramers-Kronig relation. Since optical data for the complex index of

refraction of all materials are available only for sufficiently large frequencies, at low frequencies the available data have to be supplemented with some theoretical model. When the relaxation properties of electrons in metals are taken into account, the dielectric permittivity $\varepsilon_l^{(1)}$ of our material 1 (Au) at the Matsubara frequencies can be represented in the form

$$\varepsilon_l^{(1,D)} = \frac{\tilde{\omega}_{p,1}^2}{\zeta_l(\zeta_l + \tilde{\gamma}_1)} + \varepsilon_{1,l}^{\text{cor}}. \quad (7)$$

Here, $\tilde{\omega}_{p,1}$ and $\tilde{\gamma}_1$ are, respectively, the dimensionless plasma frequency and relaxation parameter of Au connected with the dimensional ones by

$$\tilde{\omega}_{p,1} = \frac{2a\omega_{p,1}}{c}, \quad \tilde{\gamma}_1 = \frac{2a\gamma_1}{c} \quad (8)$$

and $\varepsilon_{1,l}^{\text{cor}}$ is a contribution of the core (bound) electrons to the dielectric permittivity determined by the optical data. The upper index D is used to stress that the permittivity (7) has the Drude form. Note that the relaxation parameter $\tilde{\gamma}_1$ depends on temperature and goes to zero with vanishing T by a power law for metals with perfect crystal lattices. For real metals containing some fraction of impurities there is rather small but nonzero residual relaxation at $T = 0$. For Au the values of the plasma frequency $\omega_{p,1} \approx 9 \text{ eV} = 1.37 \times 10^{16} \text{ rad/s}$ and the relaxation parameter $\gamma_1 \approx 35 \text{ meV} = 5.3 \times 10^{13} \text{ rad/s}$ have been used. If relaxation properties of free electrons are neglected, the dielectric permittivity of metals takes the plasma form

$$\varepsilon_{1,l}^p = \frac{\tilde{\omega}_{p,1}^2}{\zeta_l^2} + \varepsilon_{1,l}^{\text{cor}}. \quad (9)$$

The plasma model is usually used in the region of infrared optics where $\gamma_1 \ll \xi_l$. For the high-resistivity Si considered in this paper the extrapolation to low frequencies was done on the basis of the model

$$\varepsilon_l^{(2)} = \varepsilon_{2,l}^{\text{cor}}. \quad (10)$$

Note, that for Si $\varepsilon_{2,0}^{\text{cor}} \approx 11.67$. As mentioned above, there are puzzling results in the literature [14–19] concerning the role of dissipation of free electrons in metals. According to these results, measurements of Refs. [14–19] are in agreement with theoretical predictions of the Lifshitz theory if the available optical data of Au are extrapolated to zero frequency by means of the lossless plasma model Eq. (9) and exclude predictions of the same theory if the optical data are extrapolated by means of the theoretically better motivated Drude model Eq. (7), which takes the dissipation of free electrons into account. In our configuration, however, the

Drude-plasma dilemma makes only a negligibly small influence on the computational results [37]. We will explicitly see this in Sec. III, where we present our numerical results.

Another quantity entering Eq. (4) is the polarization tensor of graphene. At $l = 0$ the exact expressions for the polarization tensor are given by [41, 44]

$$\begin{aligned}\tilde{\Pi}_{00,0} &= \frac{\pi\alpha y}{\tilde{v}_F} + \frac{32\alpha ak_B T}{\tilde{v}_F^2 \hbar c} \left(\ln 2 - By \int_0^1 \frac{\sqrt{1-u^2} du}{e^{Byu} + 1} \right), \\ \tilde{\Pi}_0 &= \pi\alpha\tilde{v}_F y^3 - 8\alpha\tilde{v}_F y^3 \int_0^1 \frac{u^2}{\sqrt{1-u^2} e^{Byu} + 1} du,\end{aligned}\quad (11)$$

where α is the fine-structure constant, $\tilde{v}_F = v_F/c \approx 1/300$ is the reduced Fermi velocity for graphene, and $B \equiv \hbar c \tilde{v}_F / (4ak_B T)$.

For the sake of brevity, at $l \geq 1$ we present the approximate expressions for the polarization tensor at room temperature, which lead, however, to practically exact results for the Casimir free energy at separations of our interest exceeding 50 nm [44]

$$\begin{aligned}\tilde{\Pi}_{00,l} &= \frac{\alpha(y^2 - \zeta_l^2)}{\sqrt{\tilde{v}_F^2 y^2 + \zeta_l^2}} (\pi + Y_l), \\ \tilde{\Pi}_l &= \alpha(y^2 - \zeta_l^2) \sqrt{\tilde{v}_F^2 y^2 + \zeta_l^2} (\pi + Y_l),\end{aligned}\quad (12)$$

where

$$Y_l = 4 \int_0^\infty \frac{du}{e^{\pi l u} + 1} \frac{u^2}{1 + u^2}.\quad (13)$$

Note that the quantity Y_l captures the explicit dependence of the polarization tensor on the temperature for $l \geq 1$, whereas an implicit dependence on T originates from the Matsubara frequencies.

We note also that the polarization tensor takes an exact account for the nonzero relaxation properties of graphene carriers. This is seen from the fact that along the real frequency axis this tensor does have an imaginary part [58, 59] (see also Ref. [62] for another theoretical approach to the description of relaxation of charge carriers in graphene).

III. NUMERICAL RESULTS

We have performed numerical computations of the difference F_{diff} among the Casimir forces using Eqs. (2)–(5), (11) and (12). The computational results are presented in Fig. 2(a)–(d) as functions of separation. The top lines are computed at $T = 300$ K and the bottom lines at $T = 0$ K [in the latter case summation over the discrete Matsubara

frequencies in Eq. (2) is replaced by an integration along the imaginary frequency axis; the polarization tensor at $T = 0$ K is obtained from Eq. (12) by omitting the quantity Y_l]. As is seen in Fig. 2, over the entire separation range the difference F_{diff} among the thermal Casimir forces is large enough and can be measured by using already existing experimental setups [19, 49].

As we pointed out in Sec. II, the force difference F_{diff} is practically independent of the prescription used for the Au sphere, whether Drude or plasma. For example, for the separations $a_1 = 100$ nm and $a_2 = 800$ nm at $T = 300$ K the plasma prescription gives $F_{\text{diff}}(a_1) = 2344.21$ fN and $F_{\text{diff}}(a_2) = 29.0373$ fN, while with the Drude prescription we find respectively $F_{\text{diff}}(a_1) = 2345.15$ fN and $F_{\text{diff}}(a_2) = 29.0282$ fN. The reason for almost coinciding results provided by the two prescriptions is easily understood. Indeed the choice among the Drude and plasma prescriptions affects the Casimir force mainly via the TE $l = 0$ mode. Consider first the Drude prescription. With this prescription, the reflection coefficient of Au at zero frequency for TE polarization is zero, and then it follows that within the Drude prescription the $l = 0$ TE mode contributes nothing to F_{diff} , independently of the reflection coefficient of the Si plate.

Consider now the plasma prescription. With this other prescription, the $l = 0$ TE reflection coefficient of Au is different from zero:

$$r_{\text{TE},p}^{(1)}(0, y) = \frac{y - \sqrt{y^2 + \tilde{\omega}_{p,1}^2}}{y + \sqrt{y^2 + \tilde{\omega}_{p,1}^2}}. \quad (14)$$

For the uncoated half of the Si plate, according to Eq. (3), the $l = 0$ TE reflection coefficient is zero. This implies at once that the sphere-plate force F_{Si} receives no contribution from the $l = 0$ TE mode, whatever prescription is used for Au. Consider now the force F_{gr} acting on the sphere when its tip is above the graphene-coated half of the Si plate. It turns out that the zero-frequency component $\tilde{\Pi}_0$ of the polarization tensor, given in the second line of Eq.(11), is very small and according to the second of Eq. (4) this in turn implies that the $l = 0$ TE reflection coefficient of the graphene-coated half of the Si plate is nearly zero. Because of that, the $l = 0$ TE contribution to the force F_{gr} , and then to F_{diff} , is negligibly small. Summarizing the above considerations, we find that when the Drude prescription is used the contribution of the $l = 0$ TE mode to F_{diff} is zero, while with the plasma prescription it is non-zero but negligible. This explains why the force difference F_{diff} is practically insensitive

to the prescription used for Au.

In Fig. 2 we display also the force difference $F_{\text{diff}}(a, 0)$ for $T = 0$ which is computed using the zero-temperature expression for the graphene polarization tensor and the plasma model for Au. As it can be seen from Fig. 2, the thermal correction $\Delta_T F_{\text{diff}}$

$$\Delta_T F_{\text{diff}} = F_{\text{diff}}(a, T) - F_{\text{diff}}(a, 0), \quad (15)$$

which is equal to the difference between the top and bottom lines in Fig. 2, contributes to F_{diff} significantly and can be easily determined from the comparison between the measurement data and theory. As an example, at separation distances $a = 0.15, 0.2, 0.5, 1.0,$ and $1.5 \mu\text{m}$ the magnitudes of the thermal contributions $\Delta_T F_{\text{diff}}$ in F_{diff} are equal to 800, 406, 68.5, 17.5, and 7.8 fN, respectively, which are far larger than the current experimental sensitivity.

It is interesting to determine the relative weights of the different contributions which make up the thermal effect. For this purpose, we decompose the thermal correction $\Delta_T F_{\text{diff}}$ to the differential force into two parts

$$\Delta_T F_{\text{diff}}(a, T) = \Delta_T^{(1)} F_{\text{diff}}(a, T) + \Delta_T^{(2)} F_{\text{diff}}(a, T). \quad (16)$$

Here, we have introduced the notations

$$\begin{aligned} \Delta_T^{(1)} F_{\text{diff}}(a, T) &= F_{\text{diff}}(a, T) - \bar{F}_{\text{diff}}(a, T), \\ \Delta_T^{(2)} F_{\text{diff}}(a, T) &= \bar{F}_{\text{diff}}(a, T) - F_{\text{diff}}(a, 0), \end{aligned} \quad (17)$$

where $\bar{F}_{\text{diff}}(a, T)$ is calculated by Eq. (2) at $T = 300 \text{ K}$, but using the zero-temperature value for the graphene polarization tensor (keeping fixed the room temperature permittivities of Au and Si). From Eq. (17) it is clear that $\Delta_T^{(1)} F_{\text{diff}}$ originates from the explicit dependence of the graphene polarization tensor on the temperature as a parameter, whereas $\Delta_T^{(2)} F_{\text{diff}}$ represents the contribution to the thermal correction caused by the summation over the discrete Matsubara frequencies and (if the Drude model is used) by the temperature dependence of the relaxation frequency of Au. In Fig. 3 we plot the ratio $\Delta_T F_{\text{diff}}/F_{\text{diff}}$ as a function of separation (the solid line). In the same figure, the short-dashed and long-dashed lines show, respectively, plots of the ratios $\Delta_T^{(1)} F_{\text{diff}}/F_{\text{diff}}$ and $\Delta_T^{(2)} F_{\text{diff}}/F_{\text{diff}}$ (the sum of the short-dashed and long-dashed lines results in the solid one). As it can be seen in Fig. 3, the total thermal correction contributes to F_{diff} for fractions of 0.728, 0.781, 0.898, 0.946, and 0.963 at $a = 0.15, 0.2, 0.5, 1.0,$ and $1.5 \mu\text{m}$, respectively. The explicit dependence of

the polarization tensor on T by itself contributes for fractions of 0.506, 0.540, 0.613, 0.644, and 0.655 at the same respective separations. As to the thermal effect originating from the discrete summation over the Matsubara frequencies using the zero-temperature polarization tensor, it contributes smaller fractions of F_{diff} equal to 0.222, 0.241, 0.285, 0.302, and 0.308 at separations 0.15, 0.2, 0.5, 1.0, and 1.5 μm , respectively. If Au at low frequencies is described by the Drude model, this leads to only negligibly small changes in the results obtained which do not influence on the lines shown in Fig. 3.

IV. CONCLUDING REMARKS

To conclude, we have proposed a Casimir configuration allowing for an unambiguous measurement of the giant thermal effect in graphene based on already existing experimental setups. This conclusion is drawn in the framework of the Dirac model of graphene using the rigorous formalism of the polarization tensor based on the first principles of quantum electrodynamics. According to our results, both the differential force arising from the presence of a graphene coating on one half of a Si plate and the thermal contribution to it are easily observable over the considered separation region from 0.1 to 1.5 μm . We have also shown that both the explicit dependence of the material properties of graphene on the temperature, as well as the implicit temperature dependence due to summation over the Matsubara frequencies need to be taken into account when comparing experiment with theory. The obtained results open novel opportunities for the investigation of dispersion interactions in graphene systems and can be used for modulation and control of operational forces in micromechanical devices which include elements based on graphene and other 2D-materials.

Acknowledgments

The work of V.M.M. was partially supported by the Russian Government Program of Competitive Growth of Kazan Federal University.

[1] M. I. Katsnelson, K. S. Novoselov, and A. K. Geim, *Nature Phys.* **2**, 620 (2006).

- [2] M. I. Katsnelson, *Graphene: Carbon in Two Dimensions* (Cambridge University Press, Cambridge, 2012).
- [3] A. H. Castro Neto, F. Guinea, N. M. R. Peres, K. S. Novoselov, and A. K. Geim, *Rev. Mod. Phys.* **81**, 109 (2009).
- [4] S. Das Sarma, S. Adam, E. H. Hwang, and E. Rosa, *Rev. Mod. Phys.* **83**, 407 (2011).
- [5] P. Vogt, P. De Padova, C. Quaresima, J. Avila, E. Frantzeskakis, M. C. Asensio, A. Resta, B. Ealet, and G. L. Lay, *Phys. Rev. Lett.* **108**, 155501 (2012).
- [6] M. E. Dávila, L. Xian, S. Cahangirov, A. Rubio, and G. L. Lay, *New J. Phys.* **16**, 095002 (2014).
- [7] F.-f. Zhu, W.-j. Chen, Y. Xu, C.-l. Gao, D.-d. Gun, C.-h. Liu, D. Qian, S.-C. Zhang, and J.-f. Jia, *Nature Mater.* **14**, 1020 (2015).
- [8] V. A. Parsegian, *Van der Waals Forces: A Handbook for Biologists, Chemists, Engineers, and Physicists* (Cambridge University Press, Cambridge, 2005).
- [9] M. Bordag, G. L. Klimchitskaya, U. Mohideen, and V. M. Mostepanenko, *Advances in the Casimir Effect* (Oxford University Press, Oxford, 2015).
- [10] J. Hermann, R. A. Distasio, Jr., and A. Tkatchenko, *Chem. Reviews* **117**, 4714 (2017).
- [11] G. L. Klimchitskaya, U. Mohideen, and V. M. Mostepanenko, *Rev. Mod. Phys.* **81**, 1827 (2009).
- [12] A. W. Rodrigues, F. Capasso, and S. G. Johnson, *Nature Photonics* **5**, 211 (2011).
- [13] L. M. Woods, D. A. R. Dalvit, A. Tkatchenko, P. Rodrigues-Lopez, A. W. Rodrigues, and R. Podgornik, *Rev. Mod. Phys.* **88**, 045003 (2016).
- [14] R. S. Decca, D. López, E. Fischbach, G. L. Klimchitskaya, D. E. Krause, and V. M. Mostepanenko, *Phys. Rev. D* **75**, 077101 (2007).
- [15] R. S. Decca, D. López, E. Fischbach, G. L. Klimchitskaya, D. E. Krause, and V. M. Mostepanenko, *Eur. Phys. J. C* **51**, 963 (2007).
- [16] C.-C. Chang, A. A. Banishev, R. Castillo-Garza, G. L. Klimchitskaya, V. M. Mostepanenko, and U. Mohideen, *Phys. Rev. B* **85**, 165443 (2012).
- [17] A. A. Banishev, G. L. Klimchitskaya, V. M. Mostepanenko, and U. Mohideen, *Phys. Rev. Lett.* **110**, 137401 (2013).
- [18] A. A. Banishev, G. L. Klimchitskaya, V. M. Mostepanenko, and U. Mohideen, *Phys. Rev. B* **88**, 155410 (2013).

- [19] G. Bimonte, D. López, and R. S. Decca, *Phys. Rev. B* **93**, 184434 (2016).
- [20] H. B. Chan, V. A. Aksyuk, R. N. Kleiman, D. J. Bishop, and F. Capasso, *Science* **291**, 1941 (2001).
- [21] W. Broer, H. Waalkens, V. B. Svetovoy, J. Knoester, and G. Palasantzas, *Phys. Rev. Applied* **4**, 054016 (2015).
- [22] M. Sedighi, W. H. Broer, G. Palasantzas, and B. J. Kooi, *Phys. Rev. B* **88**, 165423 (2013).
- [23] J. Zou, Z. Marcet, A. W. Rodriguez, M. T. H. Reid, A. P. McCauley, I. I. Kravchenko, T. Lu, Y. Bao, S. G. Johnson, and H. B. Chan, *Nature Commun.* **4**, 1845 (2013).
- [24] G. Gómez-Santos, *Phys. Rev. B* **80**, 245424 (2009).
- [25] D. Drosdoff and L. M. Woods, *Phys. Rev. B* **82**, 155459 (2010).
- [26] Bo E. Sernelius, *Phys. Rev. B* **85**, 195427 (2012).
- [27] A. D. Phan, L. M. Woods, D. Drosdoff, I. V. Bondarev, and N. A. Viet, *Appl. Phys. Lett.* **101**, 113118 (2012).
- [28] J. F. Dobson, T. Gould, and G. Vignale, *Phys. Rev. X* **4**, 021040 (2014).
- [29] V. B. Svetovoy and G. Palasantzas, *Phys. Rev. Applied* **2**, 034006 (2014).
- [30] N. Knusnutdinov, R. Kashapov, and L. M. Woods, *Phys. Rev. A* **94**, 012513 (2016).
- [31] E. M. Chudnovsky and R. Zarzuela, *Phys. Rev. B* **94**, 085424 (2016).
- [32] D. Drosdoff, I. V. Bondarev, A. Widom, R. Podgornik, and L. M. Woods, *Phys. Rev. X* **6**, 011004 (2016).
- [33] Bo E. Sernelius, *J. Phys.: Condens. Matter* **27**, 214017 (2015).
- [34] P. Rodriguez-Lopez, W. J. M. Kort-Kamp, D. A. R. Dalvit, and L. M. Woods, *Nature Commun.* **8**, 14699 (2017).
- [35] M. Bordag, I. V. Fialkovsky, D. M. Gitman, and D. V. Vassilevich, *Phys. Rev. B* **80**, 245406 (2009).
- [36] I. V. Fialkovsky, V. N. Marachevsky, and D. V. Vassilevich, *Phys. Rev. B* **84**, 035446 (2011).
- [37] M. Bordag, G. L. Klimchitskaya, and V. M. Mostepanenko, *Phys. Rev. B* **86**, 165429 (2012).
- [38] M. Chaichian, G. L. Klimchitskaya, V. M. Mostepanenko, and A. Tureanu, *Phys. Rev. A* **86**, 012515 (2012).
- [39] G. L. Klimchitskaya and V. M. Mostepanenko, *Phys. Rev. B* **87**, 075439 (2013).
- [40] G. L. Klimchitskaya, U. Mohideen, and V. M. Mostepanenko, *Phys. Rev. B* **89**, 115419 (2014).
- [41] M. Bordag, G. L. Klimchitskaya, V. M. Mostepanenko, and V. M. Petrov, *Phys. Rev. D* **91**,

- 045037 (2015); **93**, 089907(E) (2016).
- [42] G. L. Klimchitskaya, V. M. Mostepanenko, and Bo E. Sernelius, Phys. Rev. B **89**, 125407 (2014).
- [43] G. L. Klimchitskaya and V. M. Mostepanenko, Phys. Rev. A **89**, 052512 (2014).
- [44] G. L. Klimchitskaya and V. M. Mostepanenko, Phys. Rev. A **91**, 174501 (2015).
- [45] G. Bimonte, Phys. Rev. Lett. **112**, 240401 (2014).
- [46] G. Bimonte, Phys. Rev. Lett. **113**, 240405 (2014).
- [47] G. Bimonte, Phys. Rev. B **91**, 205443 (2015).
- [48] R. S. Decca, D. López, E. Fischbach, D. E. Krause, and C. R. Jamell, Phys. Rev. Lett. **94**, 240401 (2005).
- [49] Y.-J. Chen, W. K. Tham, D. E. Krause, D. López, E. Fischbach, and R. S. Decca, Phys. Rev. Lett. **116**, 221102 (2016).
- [50] E. M. Lifshitz, Zh. Eksp. Teor. Fiz. **29**, 94 (1955) [Sov. Phys. JETP **2**, 73 (1956)].
- [51] J. Blocki, J. Randrup, W. J. Swiatecki and C. F. Tsang, Ann. Phys. (N.Y.) **105**, 427 (1977).
- [52] C. D. Fosco, F. C. Lombardo, and F. D. Mazzitelli, Phys. Rev. D **84**, 105031 (2011).
- [53] G. Bimonte, T. Emig, R. L. Jaffe, and M. Kardar, Europhys. Lett. **97**, 50001 (2012).
- [54] G. Bimonte, T. Emig, and M. Kardar, Appl. Phys. Lett. **100**, 074110 (2012).
- [55] L. P. Teo, Phys. Rev. D **88**, 045019 (2013).
- [56] L. A. Falkovsky and S. S. Pershoguba, Phys. Rev. B **76**, 153410 (2007).
- [57] T. Stauber, N. M. R. Peres, and A. K. Geim, Phys. Rev. B **78**, 085432 (2008).
- [58] G. L. Klimchitskaya and V. M. Mostepanenko, Phys. Rev. B **93**, 245419 (2016).
- [59] G. L. Klimchitskaya and V. M. Mostepanenko, Phys. Rev. B **94**, 195405 (2016).
- [60] *Handbook of Optical Constants of Solids*, ed. E. D. Palik (Academic, New York, 1985).
- [61] *Handbook of Optical Constants of Solids*, vol. 2, ed. E. D. Palik (Academic, New York, 1991).
- [62] Wang-Kong Tse and S. Das Sarma, Phys. Rev. B **79**, 235406 (2009).

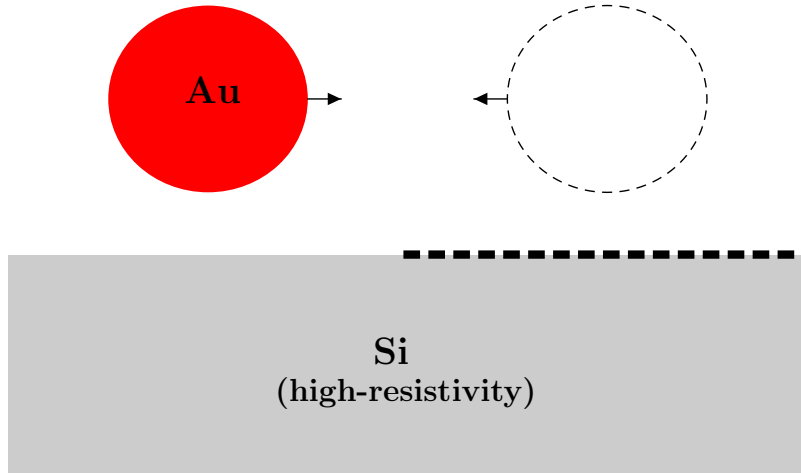


FIG. 1: The experimental configuration of a Au sphere moving back and forth above a Si plate, half of which is covered with graphene (shown by dashes). The measured quantity is the differential Casimir force F_{diff} between the Au sphere and the two halves of the plate when the sphere tip is far away from their boundaries. The figure displays the two extreme positions of the sphere during its motion. The size of the sphere is shown not to scale.

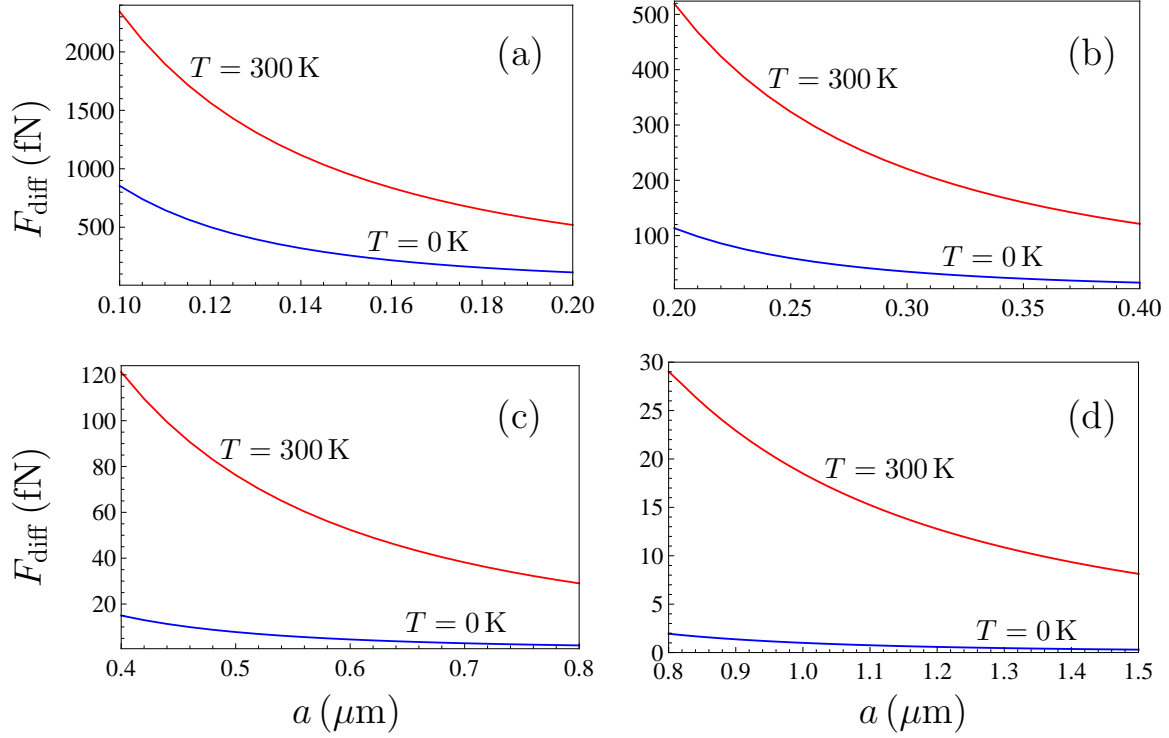


FIG. 2: The differences F_{diff} among the Casimir forces calculated at $T = 300\text{ K}$ (top lines) and at $T = 0\text{ K}$ (bottom lines) are shown as functions of separation over four different separation intervals.

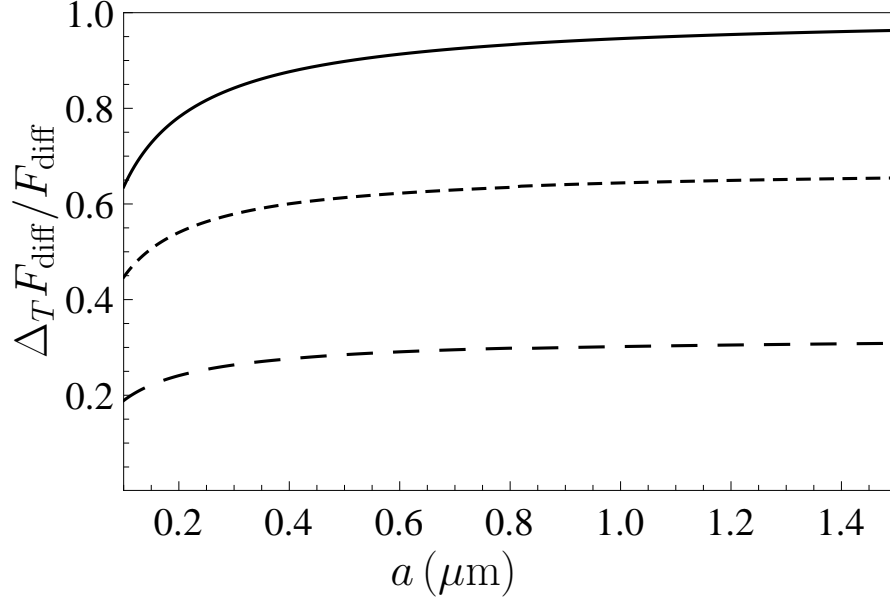


FIG. 3: The relative thermal correction $\Delta_T F_{\text{diff}}/F_{\text{diff}}$ to the difference among the Casimir forces (solid line). The short dashed line shows the relative contribution $\Delta_T^{(1)} F_{\text{diff}}/F_{\text{diff}}$ to the thermal correction arising from the explicit temperature dependence of the polarization tensor of graphene, while the long-dashed line shows the relative contribution $\Delta_T^{(2)} F_{\text{diff}}/F_{\text{diff}}$ originating from the combined effect of the temperature dependence of the Au relaxation frequency together with the implicit temperature dependence brought about by the discrete summation over the Matsubara frequencies.